Controlled Net Shape, Density, and Microstructure of TiC–NiTi Cermets Using Quasi-Isostatic Pressing

E. A. Olevsky[1], E. R. Kristofetz[2], and M.A. Meyers[3]

[1]*Institute for Mechanics and Materials, University of California,*
San Diego, 9500 Gilman Dr., La Jolla, CA 92093-0404, USA
[2]*Materials Science Group, University of California, San Diego, La Jolla, CA 92093-0418, USA*
[3]*Department of AMES, University of California, San Diego, La Jolla, CA 92093-0411, USA*

The high cost of equipment for hot and cold isostatic pressing of powder and porous materials stimulates the development of new competing technologies such as the Ceracon quasi-isostatic method (QIP). QIP has advantages when used in combination with other nonconventional processing technologies such as self-propagating high temperature synthesis (SHS). In contrast with conventional containerless isostatic pressing, considerable shape change is possible under QIP. A mathematical model of QIP is elaborated and theoretical predictions are compared to data from experiments on Ni and Ti powder compacts. Then QIP is used in combination with SHS to produce dense TiC–NiTi cermets. The possibilities of controlling net shape, final density, and phase composition are analyzed.

Key words: *combustion synthesis, SHS-densification, quasi-isostatic pressing, TiC–NiTi cermets.*

1. INTRODUCTION

Uniaxial pressing with a pressure-transmitting medium (PTM) (Fig. 1) has been attracting attention [1]. Known as the Ceracon [2] or quasi-isostatic pressing (i.e. QIP) process, it has been utilized industrially in manufacturing [3] and more recently, in combination with self-propagating high-temperature synthesis (i.e. SHS) [4–9]. When combined with SHS, QIP offers a relatively simple processing method by which hundreds of industrially-useful materials can be produced and shaped into engineering components. A granular pressure-transmitting medium (alumina or alumina with graphite powder) not only serves as a load transmitter, but also as a natural thermal insulator which prevents substantial heat loss and minimizes temperature gradients during SHS.

In light of the current development of near-net-shape technologies, the analysis of both shape and volume changes under QIP is of considerable importance. The factors which influence the shape and volume change of a porous body include the initial porosities of both the PTM and porous body, and their respective constitutive properties. The investigation of the effect of these factors on shape change during QIP is one of the objectives of this work. Section 2 is dedicated to the general model and experimental analysis of the shape evolution under quasi-isostatic pressing.

High density of the final product and the controlled phase composition resulting from the SHS-QIP processing sequence are the two other objectives of the present work. Section 3 includes experimental data on combustion synthesis and densification procedure applied to the production of TiC–Ni–Ti composites.
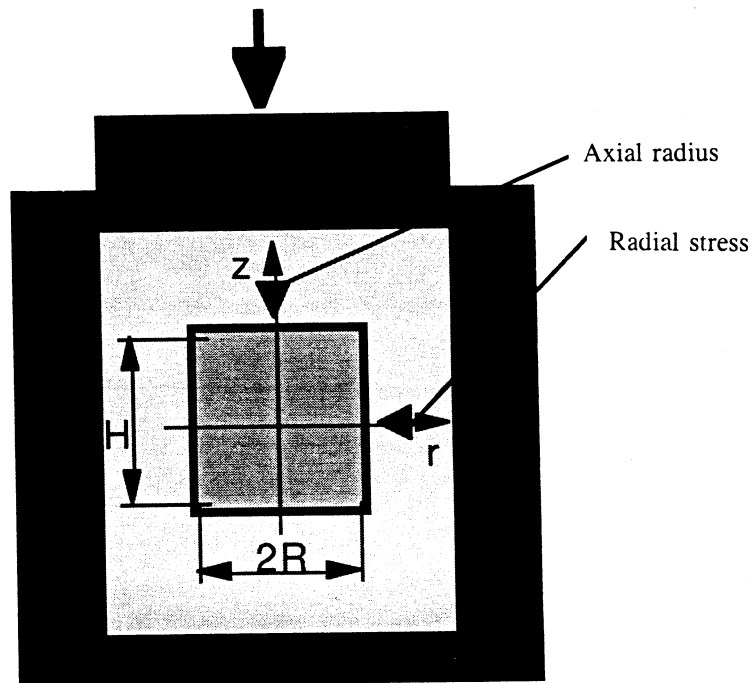

Fig. 1. Loading mode under quasi-isostatic pressing.

2. MODELING AND EXPERIMENTATION OF SHAPE CHANGE UNDER QUASI-ISOSTATIC PRESSING

2.1. Theory of Shape Change

Mechanical response of a nonlinear-viscous porous body can be described [10–12] by a rheological (constitutive) relationship connecting components of stress tensor σ_{ij} and strain rate tensor $\dot{e}_{ij}$:

$$\sigma_{ij} = A \left[\frac{\sqrt{\varphi \dot{\gamma}^2 + \psi \dot{e}^2}}{\sqrt{1-\theta}} \right]^{n-1} \left[\varphi \dot{e}_{ij} + \left(\psi - \frac{1}{3}\varphi \right) \dot{e}\delta_{ij} \right] \tag{1}$$

where A and n are material creep parameters; φ and ψ are the shear and bulk normalized viscosity module, which depend on porosity θ (for example, following [10–12], $\varphi = (1 - \theta)^2$, $\psi = \frac{2}{3}\frac{(1-\theta)^3}{\theta}$; δ_{ij} is a Kronecker symbol ($\delta_{ij} = 1$ if $i = j$, and $\delta_{ij} = 0$ if $i \neq j$); $\dot{e}$ is the first invariant of the strain rate tensor, i.e., sum of tensor diagonal components: $\dot{e} = \dot{e}_{11} + \dot{e}_{22} + \dot{e}_{33}$.

For this analysis, the constitutive behavior of the PTM is assumed to be elastic, while that of the porous body is assumed to be nonlinearly viscous. It is also assumed that the stresses are uniform within both the PTM and the porous body. For simplicity, a cylindrical geometry is assumed, and cylindrical coordinate system is used throughout this paper (Fig. 1).

In cylindrical coordinates, the volume-change rate $\dot{e}$ and the shape-change rate $\dot{\gamma}$ are given by:

$$\dot{e} = \dot{e}_{zz} + 2\dot{e}_{rr} = \left[1 + 2\left(\frac{\dot{e}_{rr}}{\dot{e}_{zz}} \right) \right] \dot{e}_{zz} = \frac{\dot{\theta}}{1-\theta} \tag{2}$$

$$\dot{\gamma} = \sqrt{\frac{2}{3}} \, |\dot{e}_{zz} - \dot{e}_{rr}| = \sqrt{\frac{2}{3}} \left| 1 - \left(\frac{\dot{e}_{rr}}{\dot{e}_{zz}} \right) \right| |\dot{e}_{zz}| \tag{3}$$

where $\dot{e}_{zz}$, $\dot{e}_{rr}$, and θ are the axial strain rate, radial strain rate, and porosity, respectively. For a cylindrical specimen, the axial and radial strain rates are given by:

$$\dot{e}_{zz} = \frac{\dot{H}}{H}; \, \dot{e}_{rr} = \frac{\dot{R}}{R} \tag{4}$$

where H and R are the instantaneous cylinder height and radius. Equation (3) gives the following relationship for the shape-change rate:

$$\dot{\gamma} = \sqrt{\frac{2}{3}} \left| \frac{\dot{H}}{H} - \frac{\dot{R}}{R} \right| \tag{5}$$

This expression will be used to derive relationships between the height and radius of the cylindrical specimen and porosity.

It is further assumed that the presence of the porous cylindrical body within the PTM provides a negligible effect on its state-of-stress as a result of the applied axial load. This is equivalent to imagining the porous cylindrical body embedded in an infinitely-extended PTM with a far-field applied stress σ_{zz}^{∞} at its boundary. The PTM itself is assumed to be under the condition of uniaxial load with lateral confinement (i.e., pressing in a rigid die). Therefore, the sample can be considered under

conditions of biaxial loading (Fig. 1).

For the PTM, the axial and radial stresses are related to the axial strain ε_{zz} by Hooke's law and are given by:

$$\sigma_{zz} = \left[\frac{1 - v}{(1 + v)(1 - 2v)} \right] E\varepsilon_{zz} \tag{6}$$

$$\sigma_{rr} = \left[\frac{1 - v}{(1 + v)(1 - 2v)} \right] E\varepsilon_{zz} \tag{7}$$

where v and E are Poisson's ratio and Young's modulus for the PTM. These depend upon PTM porosity θ_p and are given by:

$$v = \frac{2 - 3\theta_p}{4 - 3\theta_p} \tag{8}$$

$$E = 4E_o \left[\frac{(1 - \theta_p)^2}{4 - 3\theta_p} \right] \tag{9}$$

where E_0 is the Young's modulus of the granular material making up the PTM. The ratio of the axial stress to the radial stress is therefore given by:

$$\frac{\sigma_{zz}}{\sigma_{rr}} = \frac{1 - v}{v} = \frac{2}{2 - 3\theta_p} = k \tag{10}$$

The following expression for the axial/radial stain-rate ratio is valid:

$$\frac{\dot{e}_{zz}}{\dot{e}_{rr}} = \frac{k(2 - 3\theta) - 2}{2(2 - 3\theta) - k(4 - 3\theta)} \tag{11}$$

If $k = \dfrac{2}{2 - 3\theta}$ (which means that $\theta = \theta_p$), then $\dot{e}_{rr} = 0$, and we have the conditions of pressing in a rigid die. If $k = 1$ (i.e., if $\theta_p = 0$ which means that PTM is an incompressible material), $\dot{e}_{rr} = \dot{e}_{zz}$, and we have the conditions of isostatic pressing. If $k \rightarrow \infty$ (i.e., if $\theta_p = 2/3$), which approximately corresponds to the density of packed isometric spherical particles, then $\dot{e}_{rr} = \dfrac{3\theta - 2}{4 - 3\theta}\dot{e}_{zz}$, and we have the conditions of free up-setting.

Combining Eqs. (2), (4), and (11) gives the following expression for the axial strain rate in terms of the rate-of-change of porosity:

$$\dot{e}_{zz} = \frac{\dot{H}}{H} = \frac{1}{3} \left[\frac{2\theta_p + (1 - 3\theta_p)}{(1 - \theta_p)(1 - \theta)} \right] \frac{\dot{\theta}}{\theta} \tag{12}$$

Combining Eqs. (2), (11), and (12) gives the following expression for the radial strain rate in terms of the rate-of-change of porosity:

$$\dot{e}_{rr} = \frac{\dot{R}}{R} = \frac{1}{3} \left[\frac{\theta - \theta_p}{(1 - \theta_p)(1 - \theta)} \right] \frac{\dot{\theta}}{\theta} \tag{13}$$

The shape rate can be represented as follows:

$$\dot{\gamma} = 2\sqrt{6} \left| \frac{(1 - \theta)(1 - k)}{2(2 - 3\theta) - k(4 - 3\theta)} \right| |\dot{e}_{zz}| \tag{14}$$

Subtracting Eq. (13) from Eq. (12), and integrating gives the following expression for the aspect ratio *H/R*:

$$\frac{\dot{H}}{H} - \frac{\dot{R}}{R} = \left(\frac{\theta_p}{1 - \theta_p} \right) \frac{\dot{\theta}}{\theta} \Rightarrow \int_{\frac{R_0}{R_0}}^{\frac{H}{R}} d\ln\left(\frac{H}{R} \right) = \left(\frac{\theta_p}{1 - \theta_p} \right) \int_{\theta_0}^{\theta} d\ln\theta \Rightarrow \frac{H}{R} = \frac{H_0}{R_0} \left(\frac{\theta}{\theta_0} \right)^{\frac{\theta_p}{1 - \theta_p}} \tag{15}$$

In deriving Eq. (15), it was assumed that θ_p is constant. Equation (15) indicates that the change in the aspect ratio *H/R* does not depend upon the constitutive behavior of either the PTM or densified body, but depends only on the PTM's porosity and the body's initial density and dimensional parameters.

In Fig. 2, the curves for various PTM porosities are shown, corresponding to the relationships between the change of the aspect ratio expressed by the relationship $\dfrac{H}{R} \Big/ \dfrac{H_0}{R_0}$ and the sample's porosity. For comparison, the curves corresponding to the conditions of free up-setting, pressing in a rigid die $\left(\dfrac{\dot{e}_{rr}}{\dot{e}_{zz}} = 0 \right)$, and isostatic pressing $\left(\dfrac{\dot{e}_{rr}}{\dot{e}_{zz}} = 1 \right)$ are shown too. Initial porosity of the sample is assumed to be $\theta_0 = 0.3$.

The calculation results indicate that, for sufficiently dense PTM, having porosity $\theta_p < 0.2$, the deformation state under QIP is close to the isostatic one. However, for most cases, in the capacity of
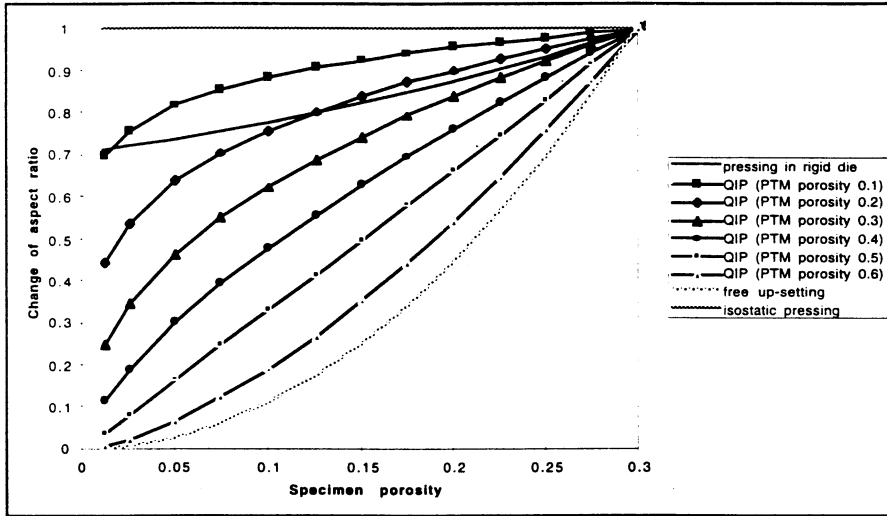

Fig. 2. Shrinkage anisotropy as a function of specimen porosity under QIP.

E. A. Olevsky, E. R. Kristofetz, and M. A. Meyers

Table 1 Evolution of aspect ratio under QIP: Comparison
of theoretical and experimental data.

	Initial height, m	Initial diameter, m	Final height, m	Final diameter, m	Initial porosity	Final porosity	Final aspect ratio (experiment)	Final aspect ratio (theory)	Relative error
Nickel	0.030	0.032	0.026	0.032	0.47	0.38	1.620	1.564	0.070
Nickel	0.012	0.032	0.010	0.032	0.48	0.35	0.610	0.580	0.102
Nickel	0.016	0.032	0.011	0.032	0.51	0.28	0.692	0.594	0.282
Titanium	0.025	0.032	0.022	0.032	0.52	0.46	1.352	1.376	0.036
Titanium	0.038	0.032	0.031	0.032	0.50	0.38	1.924	1.890	0.036
Titanium	0.025	0.032	0.021	0.032	0.45	0.35	1.282	1.242	0.064

PTM, industrial sand (alumina) or graphite powder in a loose state are used. Therefore usually $\theta_p >$ 0.2. This means that the aspect ratio evolution under QIP can be close to the one obtained under the conditions of pressing in a rigid die or free up-setting.

2.2. Experimental Measurements of Shape Change

Nickel and titanium samples were produced by the preliminary cold pressing of loose powders. Cold pressing was performed to produce three nickel and three titanium samples, whose heights and diameters are given in Table 1.

In order to vary the yield limit, samples were preheated to a variety of temperatures. Each sample was then placed in a thick walled cylinder (inner diameter = 3", height = 4") and surrounded by a pressure transmitting medium. The samples were loaded under forces ranging from 2.5 to 10 kN. Diameter and height were measured before and after QIP. The results of the experiments are represented in Table 1.

Based on the experimental data on initial parameters (aspect ratio and porosity) for QIP of Ni and Ti powder samples, the calculations were performed in conformity to Eq. (15). The final aspect ratio was determined from the final height and diameter. PTM (graphite powder) porosity was determined experimentally: $\theta_p = 0.4$. This value was used in the calculations.

The experimental and theoretical data are given in Table 1. One can see that the experimental and calculation results agree well: for most cases, the relative error in values of the final aspect ratio is smaller than 5%. Thus, Eq. (15) can be recommended for use as a practical means for the quantitative prediction of the shape change during QIP.

3. QUASI-ISOSTATIC PRESSING OF SHS-PRODUCED TiC–NiTi CERMETS

Highly exothermic reactions that become self-sustaining and propagate as a combustion wave provide an attractive low-cost alternative for the production of refractory ceramics and composites. Unlike sintering, which requires heating for long periods at high temperatures, combustion synthesis uses an external energy source only for local ignition, and the reaction is complete within seconds. It has been shown that when this technique is combined with external pressure, dense products can be formed from reactant powders. For this study, TiC–Ni–Ti composites were made by combustion synthesis and densification in a granular pressure transmitting medium.
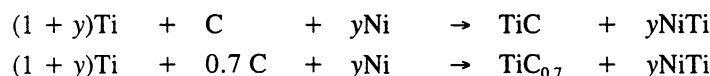
TiC–Ni–Ti composites allow for optimization of material properties by combining the hard, wear resistant properties of ceramics with the increased ductility of the metal phases. Cracks initiated in the carbide phase can be arrested by blunting of the crack tip when it reaches the more plastic Ni–Ti binder. If the binder is composed of the NiTi (1:1) phase with a CsCl structure, crack growth can also be inhibited by a stress induced martensitic transformation. The volume increase of NiTi associated with such a phase transformation creates compressive stresses at the crack tip.

3.1. Synthesis and Densification Procedure

In these combustion-densification experiments on TiC–Ni–Ti composites, the final microstructure and phase distribution were studied as a function of the initial chemical composition.

The starting materials used in this investigation were high purity powders of Ti, C, and Ni. The Ti powder (99.7% pure) from Micron Metals was classified as -325 mesh with the smallest dimension being less than 44 μm. The C powder (99.9% pure) from Consolidated Astronautics had a particle size of 2 μm with a flake-like morphology. It tended to form large agglomerates on the order 50 μm. The Ni powder (99.7% pure) from Aldrich Chemical Co. had an average particle size of 3 μm with a filament structure.

The following basic reactions were studied:

$$(1 + y)\text{Ti} \quad + \quad \text{C} \quad + \quad y\text{Ni} \quad \rightarrow \quad \text{TiC} \quad + \quad y\text{NiTi}$$
$$(1 + y)\text{Ti} \quad + \quad 0.7\,\text{C} \quad + \quad y\text{Ni} \quad \rightarrow \quad \text{TiC}_{0.7} \quad + \quad y\text{NiTi}$$

Powder was mixed in order to obtain final product compositions corresponding to volume fractions of NiTi between 0.1 and 0.5. Since sintered TiC–NiTi composites [13, 14] typically have a lattice parameter of 4.32×10^{-4} μm, which corresponds to $\text{TiC}_{0.7}$, samples were also prepared anticipating nonstoichiometric carbide.

The powders were loaded under argon into polyethylene jars and dry mixed with burundum™ grinding media (4:1 by weight) for at least 24 hours. Then they were baked in a vacuum oven for a minimum of 24 hours at approximately 100°C and under a pressure less than 100 mm Hg to remove adsorbed water. After baking, the powders were uniaxially pressed in a steel die into either 25 g or 100 g green compacts.

To aid the initiation of a planar combustion wave, the sample was placed beneath a pressed pellet of Ti and C powder and a layer of loose Ti + C reactant powder. An electrochemical match crack consisting of Ni–Cr or Sn–Cu wire wrapped around a wooden match stick head was then buried in the loose powder and ignited remotely by a variable transformer. Ignition of samples that were not subject to post-reaction densification was performed in an enclosed reaction chamber that was evacuated to approximately 50 mm Hg and backfilled with argon gas to 810 mm Hg.

The experimental configuration for the synthesis/densification process is shown in Fig. 3. The fixture used to contain the samples during processing was a thick walled steel cylinder filled with an alumina-based granular medium from Superior Graphite. 3/4"–2" of this medium was placed on the bottom of the die, and the sample was surrounded by it.

It is important to note that there is a time window for successful densification of combustion synthesized materials. For pure TiC this window corresponds to the time between when the reaction is complete and when the temperature of the sample falls below the ductile to brittle transition temperature. Adding Ni to the reaction systematically lowers the adiabatic temperature. This detrimental loss of temperature is offset, however, by the melting of the NiTi. Liquid NiTi surrounds the solid TiC spherical particles until approximately 1310°C and aids consolidation. In this study, the
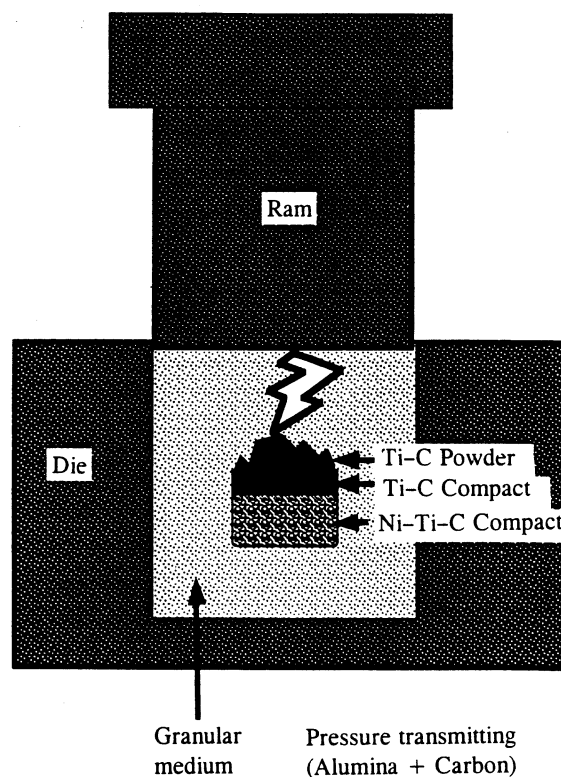
Fig. 3. Containment fixture for synthesis/densification experiments.

time delay between ignition and maximum loading was 15 sec. Densification was accomplished using the Enerpac H-frame 100 ton capacity hydraulic press. Samples were loaded to 10 tons and held at that load for 15 seconds. After densification, samples were placed in vermiculite for slow cooling.

Samples were sectioned for optical microscopy, X-ray diffraction analysis, and scanning electron microscopy. The samples were cut into longitudinal sections and mechanically ground and polished down to 1 μm. The final steps involved hand polishing with a 1/4 μm diamond paste and then a solution of colloidal SiO_2 and Al_2O_3.

3.2. Results

As-Reacted Material

Propagation of the reaction in all samples reacted in the combustion chamber was by a stable, planar wavefront. Since the samples were unconfined, gas evolution of volatile impurities resulted in lateral escape channels and longitudinal expansion. This, combined with the typical volume decrease during the reaction and the initial porosity of the reacting mixture, leads to an open network of voids. The fractional height change varied with composition as shown in Fig. 4. The longitudinal growth decreased with increasing volume fraction of NiTi until 30% NiTi and then increased with further additions. Optical microscopy, performed on a Nikon Epiphot microscope, revealed that sample porosity typically exceeds 50%.
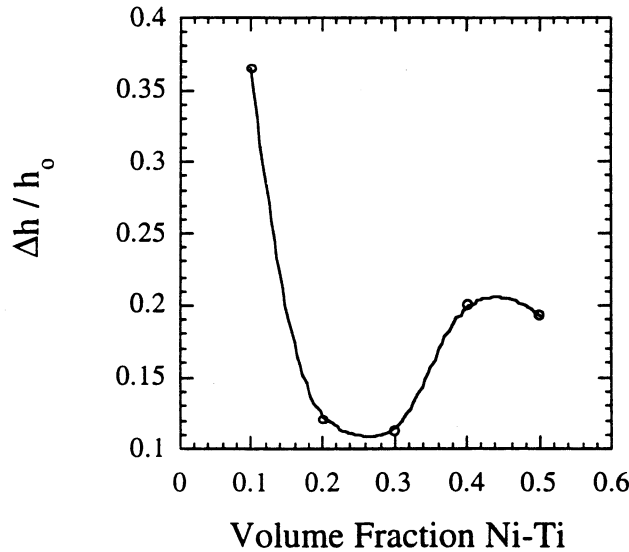
Fig. 4. Fractional height change of undensified material as a function of composition.

The hard TiC particles form spheroidal grains which are surrounded by a fairly continuous Ni–Ti layer as shown. The TiC particle size decreases with increasing volume fraction of NiTi. As mentioned above, the addition of NiTi lowers the adiabatic temperature, because the formation of NiTi from elemental powders ($\Delta H^0_{f,NiTi} = -66.5 \; Kjmol^{-1}$) does not provide as much exothermic heat, as does the formation of TiC ($\Delta H = -184.1 \; Kjmol^{-1}$). Lowering the temperature reduces Ostwald ripening.

X-ray diffraction analysis was performed in an attempt to determine the structure and composition of the cermets. The scans were performed using CuKα radiation with a Scintag XRD-2000 Theta-Theta diffractometer. The 2 Θ angles considered were between 35 and 80, with a step increment of 0.1. Figure 5 shows the diffraction peaks for TiC-40 vol% NiTi. Comparison with the JCPDS Powder Diffraction File confirms the presence of TiC and Ni_3Ti.
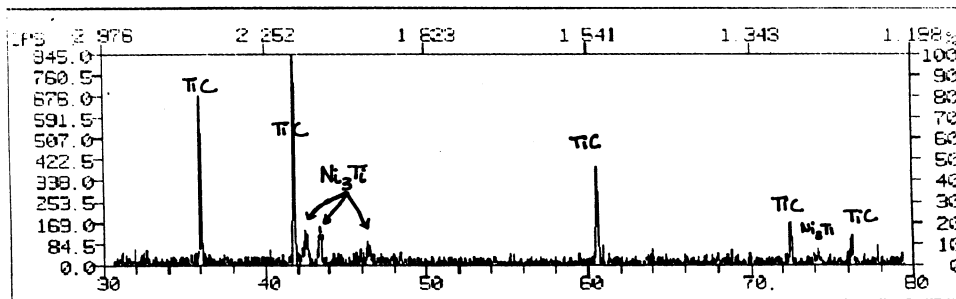

Fig. 5. X-ray diffraction pattern for stoichiometric TiC-40 volume % NiTi.

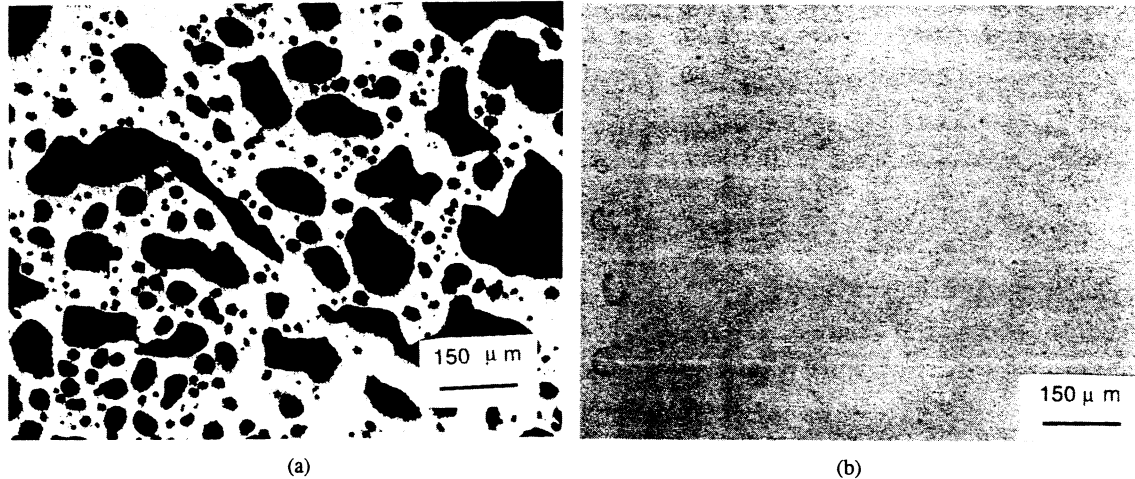(a)   (b)

Fig. 6. Microstructure of (a) as-reacted and (b) quasi-isostatically pressed TiC-40 volume % NiTi cermet.

QIPed Material

To improve the final product density, SHS was combined with densification in a pressure transmitting medium. Figures 6(A) and (B) compare the results of as-reacted and QIPed material, respectively. The average porosity was determined using a computer software program by Media Cybernetics called "Image Pro-Plus." Once an image was acquired by the computer, the threshold for material phases was set manually to match the observed contrast between regions. The average porosity was calculated from 10 different images acquired along the longitudinal cross section of the sample. This technique gave a porosity value of about 1-2% for the QIPed material.
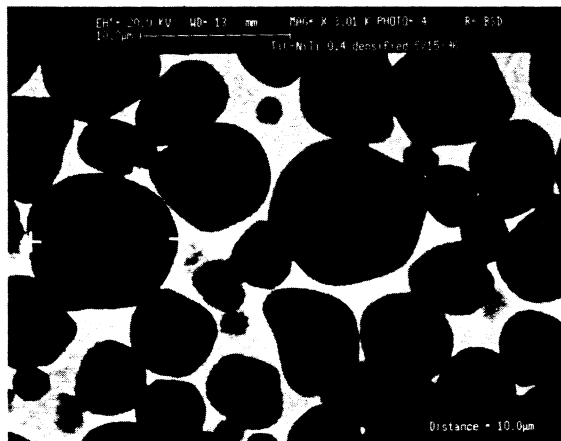

Fig. 7. Eutectic structure of binder in stoichiometric TiC-40 volume % NiTi.
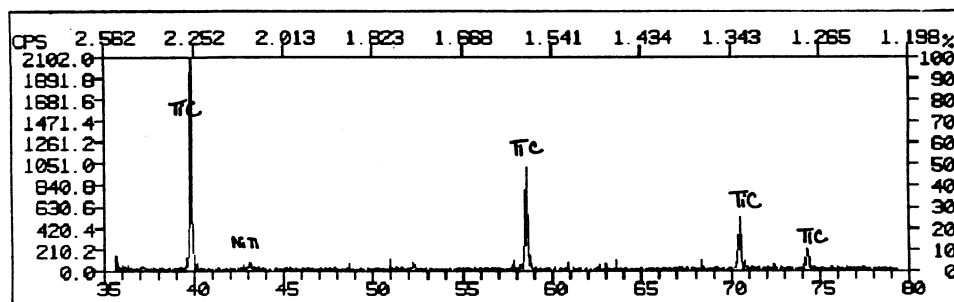
Fig. 8. X-ray diffraction pattern for non-stoichiometric $TiC_{0.7}$-40 volume % NiTi.

In several of the samples, the Ni–Ti binder appeared to be composed of two phases. Scanning electron microscopy, performed on a Cambridge 360 microscope, revealed a eutectic structure as shown in Fig. 7. According to the Ni–Ti–C ternary phase diagram [15], there is a field of three phase equilibrium, where TiC coexists with Ni_3Ti and NiTi. Studies on sintered TiC–NiTi [13, 14] have revealed that there is a redistribution of Ti atoms from the binder to the carbide. This process leads to titanium impoverishment in the binder, and consequently, to the formation of Ni_3Ti.

TiC is a cubic compound (sodium chloride structure) with an extraordinarily wide composition range. This wide range is caused by defects in the carbon sublattice resulting from the slow rate of diffusion of carbon through TiC. X-ray diffraction measurements of combustion synthesized materials mixed to obtain stoichiometric TiC–NiTi composites revealed the presence of nickel rich Ni–Ti phases. Ni_3Ti was continually the dominant binder phase. These results were thought to be the result of the formation of nonstoichiometric (titanium enriched) carbide.

In an attempt to suppress the formation of Ni_3Ti, samples were prepared with additional titanium. Powder was mixed anticipating nonstoichiometric titanium carbide, and cylindrical compacts were reacted and densified in the same manner as above. Figure 8 shows the X-ray diffraction pattern for 40% NiTi–$TiC_{0.7}$. All peaks corresponding to Ni_3Ti have disappeared.

CONCLUSIONS

1. A mathematical model of the quasi-isostatic pressing (QIP) is developed.

2. The model predicts an essential shape change under QIP for large porosities of the pressure transmitting medium (PTM).

3. The ratio between the sample and the PTM porosities influences the evolution of the integral aspect ratio.

4. A comparison of the experimental and calculation results on QIPing Ni and Ti powders demonstrates good quantitative correspondence.

5. Dense TiC–NiTi cermets can be produced by a combined SHS/QIP process.

6. The formation of Ni_3Ti in TiC–NiTi cermets can be suppressed if powder is mixed anticipating nonstoichiometric carbide.

REFERENCES

[1]   R. M. German, *Powder Metallurgy Science*, 2nd ed., Metal Powder Industries Federation, Princeton, New Jersey, 1994.

[2] R. V. Raman, S. V. Rele, S. Poland, J. LaSalvia, M. A. Meyers, and A. R. Niiler, "The one-step Synthesis of Titanium-Carbide Tiles," *J. Metals*, no. 3, pp. 23–25, 1995.

[3] M. Ohyanagi, M. Fukushima, and M. Koizumi, "TiC–TiAl Composite Fabricated SHS - Dynamic Pseudo-Isostatic Compaction Through Sand Medium," *Proc. of the Int. Conf. on Hot Isostatic Pressing*, Andover MA, pp. 289–294, 1996.

[4] P. H. Shingu, K. N. Ishihara, F. Ghonome, T. Hyakawa, M. Abe, and K. Tagushi, *Proc. of the 1st US-Japan Workshop on Combustion Synthesis* (Tsukuba), pp. 65–71, 1990.

[5] Y. V. Bogatov, E. Levashov, and A. N. Pityulin, "Effect of Special Features of the SHS Process on the Structure of Dense Titanium Carbide," *Sov. Powder Metallurgy*, 7(343), pp. 76–78, 1991.

[6] B. Mihelic, M. Dikic, R. Djekic, and D. Uskokovic, "Processing of Compact Materials by the Use of Self-Propagating High-Temperature Synthesis and Pseudo-Hot Isostatic Pressing," *Materials Letters*, vol. 13, pp. 391–395, 1992.

[7] J. C. LaSalvia and M. A. Meyers, "Microstructure, Properties, and Mechanisms of TiC–Mo–Ni Cermets Produced by SHS," *Int. J. SHS*, vol. 4, pp. 43–57, 1995.

[8] J. C. LaSalvia, D. K. Kim, R. A. Lipsett, and M. A. Meyers, "Combustion Synthesis in the Ti–C–Ni–Mo System: I. Macrokinetics and micromechanisms," *Met. Mat. Trans. A*, vol. 26A, pp. 3001–9, 1995.

[9] J. C. LaSalvia and M. A. Meyers, "Combustion Synthesis in the Ti–C–Ni–Mo system: II. Analysis," *Met. Mat. Trans. A*, vol. 26A, pp. 3011–19, 1995.

[10] V. Skorohod, E. Olevsky, and M. Shtern, "Continuum Theory of Sintering I. Phenomenological Model. Analysis of the External Forces Influence on the Sintering Kinetics," *Powd. Metall. & Met. Ceram.*, N1(361), pp. 22–27, 1993.

[11] V. Skorohod, E. Olevsky, and M. Shtern, "Continuum theory of sintering II. Effect of the rheological properties of the solid phase on the sintering kinetics," *Powd. Metall. & Met. Ceram*, N2(362), pp. 16–21 1993.

[12] E. Olevsky, H. J. Dudek, and W. A. Kaysser, "HIPing Conditions for Processing of Metal Matrix Composites Using Continuum theory for sintering I. Theoretical analysis," *Acta Met. Mater.*, vol. 44, no. 2, pp. 707–713, 1996.

[13] T. M. Poletika, S. N. Kul'kov, and V. E. Panin, "Structure, Phase Composition, and Character of Fracture of Sintered TiC–NiTi Composite Materials," *Poroshkovaya Metallurgiya*, no. 7(247), pp. 54–59, 1983.

[14] S. N. Kul'kov, T. M. Poletika, A. Yu. Chukhlomin, and V. E. Panin, "Influence of the Phase Composition of TiC–NiTi Composite Materials on the Character of Failure and Mechanical Properties," *Poroshkovaya Metallurgiya*, no. 8(260), pp. 88–92, 1984.

[15] E. R. Stover and J. Wulff, "The Nickel-Titanium-Carbon System," *Trans. Metall. Soc. AIME*, vol. 215, pp. 127–136, 1959.